

**Structure, Volume 27**

**Supplemental Information**

**Multisystem Proteinopathy Mutations**

**in VCP/p97 Increase NPLOC4·UFD1L**

**Binding and Substrate Processing**

**Emily E. Blythe, Stephanie N. Gates, Raymond J. Deshaies, and Andreas Martin**

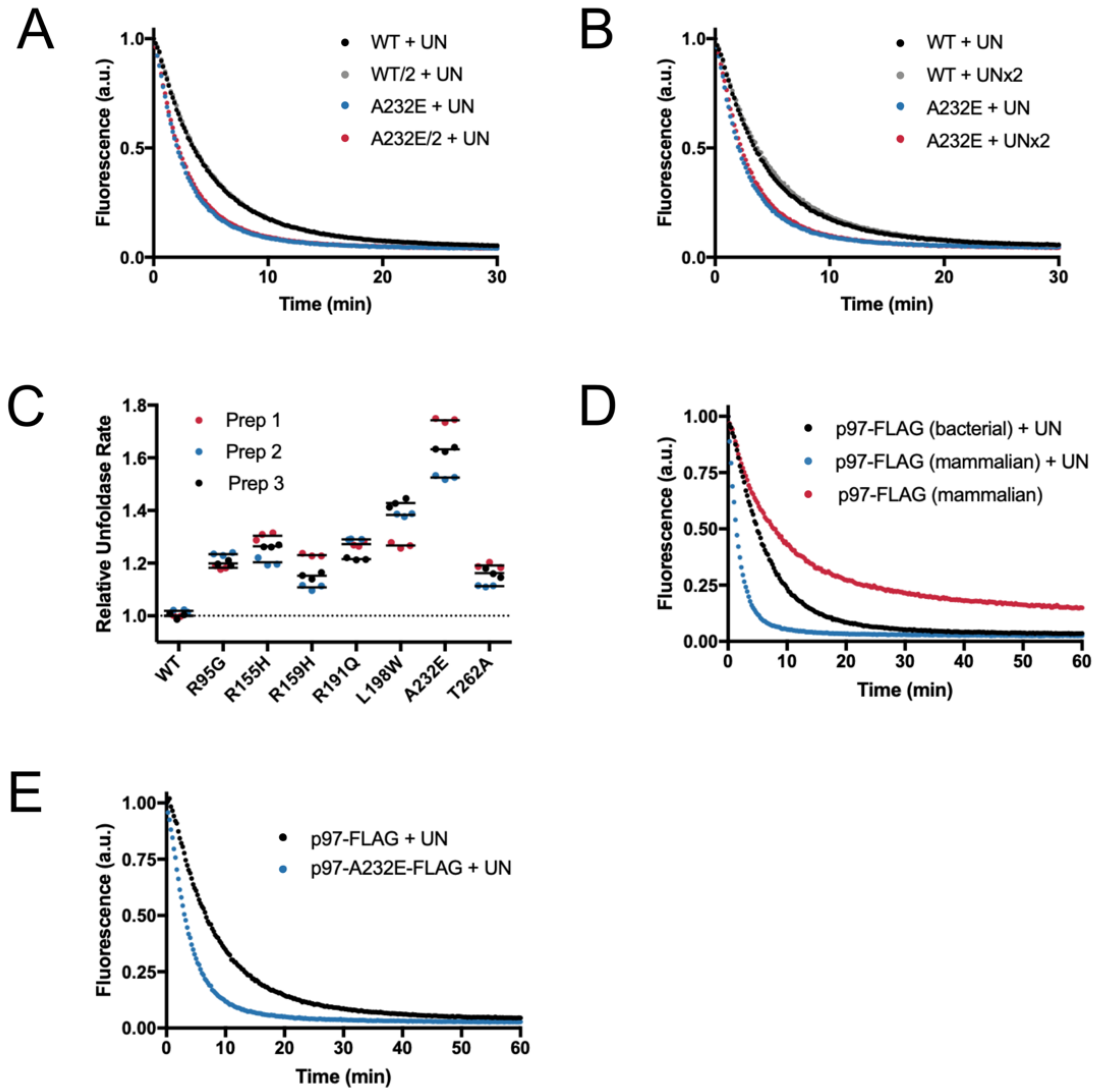


**Figure S1. Related to Figure 1. (A)** Example time courses of unfolding of split mEos3.2 show little change in normalized rate when the concentration of p97 is halved (WT:  $0.985 \pm 0.005$ , p97-A232E:  $0.937 \pm 0.006$ ). **(B)** Example time courses show little change in normalized rate when UN is doubled (WT:  $0.927 \pm 0.002$ , p97-A232E:  $0.93 \pm 0.01$ ). **(C)** Prep-to-prep variability in the unfoldase rates of MSP-mutant p97. All MSP mutants showed increased unfoldase rates compared to wild type yet with considerable prep-to-prep variabilities. For Preps 1 and 2, assays were carried out in a modified assay buffer under slightly different conditions (see Methods), and substrate-unfoldase rates were normalized to that of wild-type p97 Prep 1. The rates for the Prep 3 are replotted from Figure 1C. **(D)** Example mEos3.2 substrate-unfolding traces show that human cell-line expressed p97 in complex with UN (blue trace) is a faster unfoldase than *E. coli*-expressed p97-UN (black trace) and can promote unfolding even without the addition of exogenous UN (red trace). **(E)** Example unfolding traces show human cell-line expressed p97-A232E unfolds substrate faster than similarly expressed wild-type p97. Representative traces shown. Technical replicates,  $n \geq 2$ ,  $\pm$  S.D..

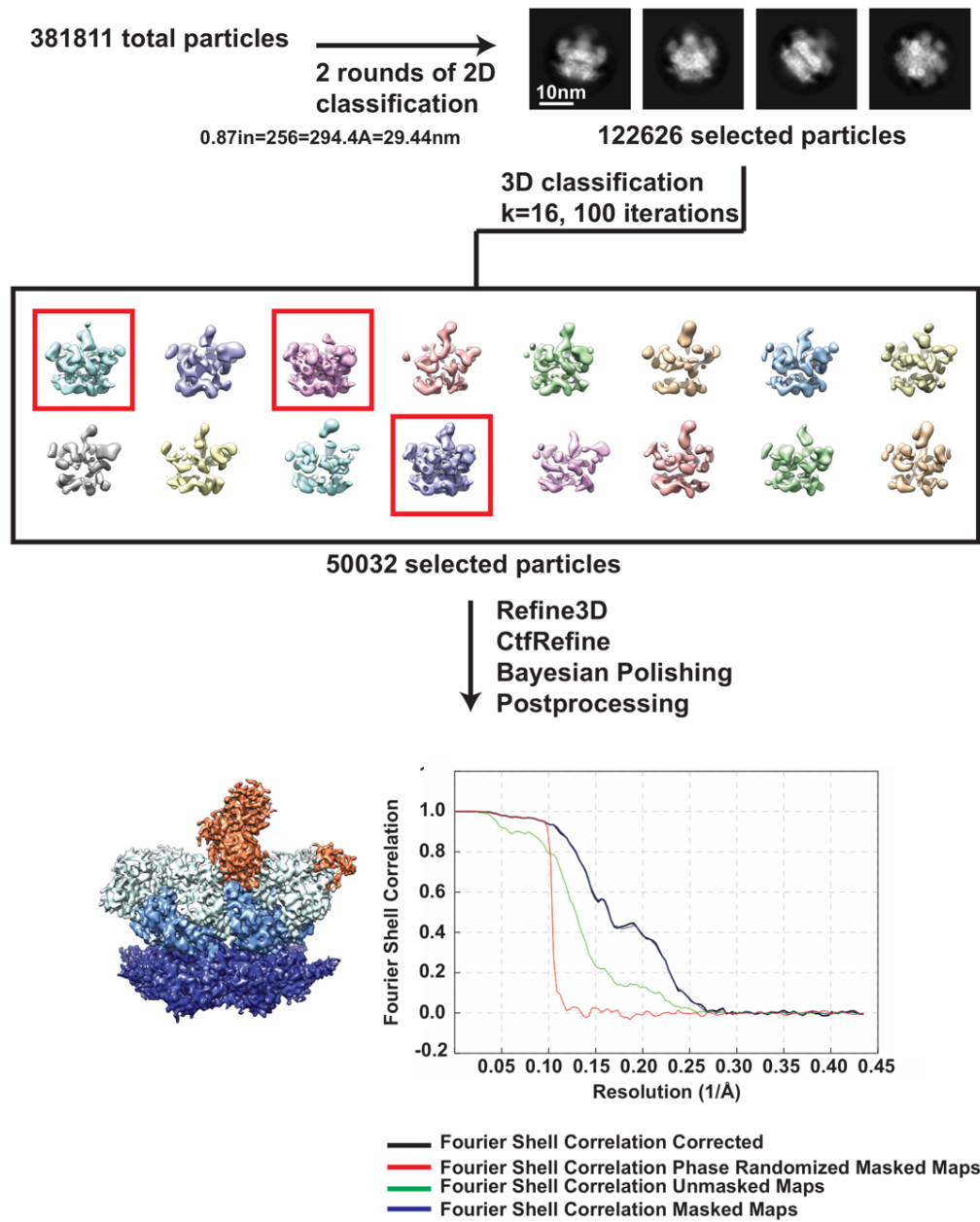


**Figure S2. Related to Figure 3.** Analysis and cryo-EM processing of the p97-A232E:UN-ATP complex. Total particles of p97-A232E:UN-ATP complex dataset were subjected to two rounds of reference-free 2D class averages to clean out contamination or bad particles, followed by a 3D classification into 16 classes. The three best classes of particles were selected from the total 16 classes (red box), resulting in a final dataset of 50,032 particles. This particle stack was refined with CtfRefinement, Bayesian polishing, and post-processing, resulting in a final resolution of 4.26Å, evaluated using gold standard FSC curves of the masked and unmasked post-processed final reconstructions (Scheres, 2012). The final map is colored by domains: NPLOC4 (orange), NTDs (light blue), D1 (sky blue), D2 (navy blue).

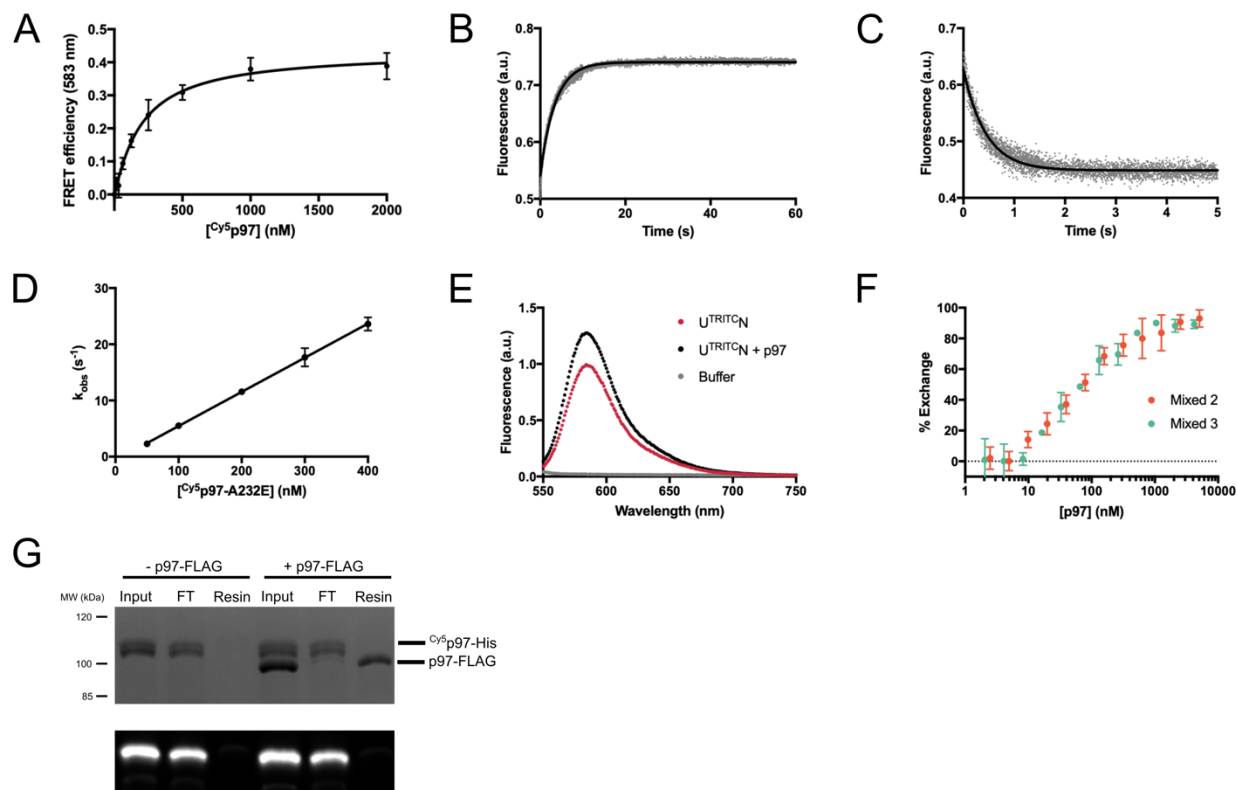


**Figure S3. Related to Figure 5 and Table 1. (A)** Example FRET-based binding curve for the interaction of U<sup>TRITCN</sup> with variable concentrations of <sup>Cy5</sup>p97 in ATPγS. Data were fit to a quadratic binding equation (technical replicates, N = 3, ± S.D.). **(B)** Example trace and single-exponential fit for the dissociation of U<sup>TRITCN</sup> from <sup>Cy5</sup>p97 in ATPγS, measured by the recovery of donor TRITC fluorescence after stopped-flow mixing. **(C)** Example trace and single-exponential fit for the binding of U<sup>TRITCN</sup> to <sup>Cy5</sup>p97 in ATPγS, measured by the quenching of donor TRITC fluorescence after stopped-flow mixing. **(D)** Shown are the observed rate constants  $k_{obs}$  for the association of U<sup>TRITCN</sup> with <sup>Cy5</sup>p97-A232E in ATPγS, derived from single-exponential fits of binding kinetics at various <sup>Cy5</sup>p97-A232E concentrations. The association rate constant,  $k_{on}$ , was determined by linear regression (technical replicates, N ≥ 5, ± S.D.). **(E)** U<sup>TRITCN</sup> fluorescence (red, 50 nM) is sensitive to binding of unlabeled p97 (black, 2.5 μM). **(F)** Competition FRET experiment, monitoring the dissociation of U<sup>TRITCN</sup> from Cy5-labeled p97-A232E and binding to excess unlabeled Mixed 2 and Mixed 3 heterohexamers, show that the mixed heterohexamers have similar UN affinities (technical replicates, N ≥ 2, ± S.D.). **(G)** Protomer exchange between p97 hexamers is slow. Coomassie stain and fluorescence scan of an SDS-PAGE gel show no evidence of His-tagged <sup>Cy5</sup>p97 binding to the anti-FLAG resin despite robust binding of FLAG-tagged p97.

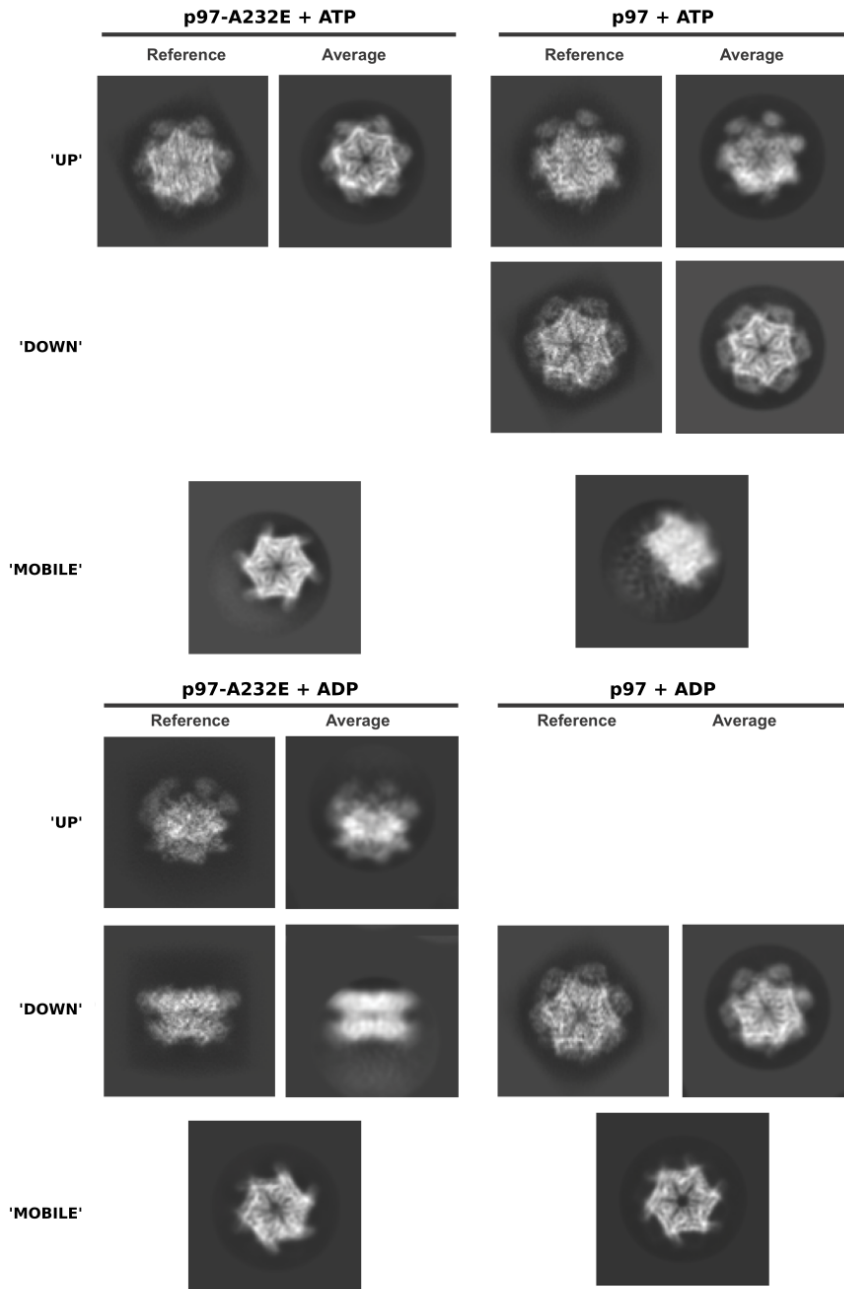


**Figure S4: Related to Figure 6.** Representative 2D class averages of nucleotide datasets, compared to back projections of 3D models. Back projections of the 3D models for p97-ATP $\gamma$ S (EMD:3297) and p97-ADP (EMD:3299) (Banerjee et al., 2016) next to a representative 2D class average from each nucleotide dataset, oriented in the same angle. Representative averages are also shown for hexamers with 'mobile' NTDs.

	p97-A232E-UN:ATP	p97-ATP	p97-A232E-ATP	p97-ADP	p97-A232E-ADP
<b>Microscope</b>	Titan Krios	Talos Arctica			
<b>Nominal Mag.</b>	33,333x	43,860x			
<b>Detector</b>	K2			K3	
<b>Pixel Size (Å/pixel)</b>	1.15	1.16		1.14	
<b>Exposure (s)</b>	8			5.273	
<b>Frame rate (s)</b>	0.2			0.12	
<b>Total electron dose</b>	48				
<b>Defocus Range (µm)</b>	-1 to -2.5				
<b>Total Micrographs</b>	5897	1100	704	706	1781
<b>Total Particles</b>	164673	170204	141281	414495	181424

**Table S1. Related to Figure 3 and Figure 6. Parameters for the cryo-EM data collection.**